








Tri-Band, Stable and Compact Patch Frequency Selective Surface Optimized via Hybrid Bioinspired Computing for Applications at 2.4, 3.5 and 5.8 GHz

Flávio H. C. S. Ferreira¹ , Jasmine P. L. Araújo¹ , Alfredo Gomes Neto² , Ianes B. G. Coutinho² , Fabrício J. B. Barros¹ , Gervásio P. S. Cavalcante¹ , Miércio C. de Alcântara Neto¹ 

¹Institute of Technology, Federal University of Pará, Brazil, henryferreira014@gmail.com, jasmine@ufpa.br, fbarros@ufpa.br, gervasio@ufpa.br, miercio@ufpa.br

²Federal Institute of Education, Science and Technology of Paraíba, Brazil, alfredogomesjpa@gmail.com, ianesgrecia@gmail.com

Abstract— This work addresses the synthesis of a multi-band frequency selective surface (FSS) through bioinspired computing and a general regression neural network (GRNN). This hybrid computational method, which utilizes the multi-objective cuckoo search algorithm combined to a GRNN, determine the best physical dimensions of the FSS in order to achieve a multi-band filtering at the 2.4, 3.5 and 5.8 GHz spectrums. Therefore, the results are to be applied to aid the propagation of Wi-Fi, WLAN, WiMAX and future sub-6 GHz 5G systems. The resonant frequencies were measured and a -10 dB cutoff value has been considered for the transmission coefficient. The triple rectangular loop conductor geometry of the device is printed upon a glass epoxy (FR-4) substrate. Measurements were made for different wave incidence angles, from 0° up to 45°, to demonstrate how signal incidence would affect the device's functioning. The agreement between simulated and measured data display satisfactory results.

Index Terms— Multi-band FSS, 5G, optimization, GRNN, MOCS.

I. INTRODUCTION

The fifth generation of wireless communication, or 5G system, is being currently planned out, and there are many papers in the literature focusing on proposing operating frequency spectrums and propagation applications in order to make 5G systems function. According to [1], 5G operation aims for a 1,000 times greater traffic capacity, and an extended bandwidth capacity able to work at 1ms latency response with data rates in the order from 1 Gbps up to 10 Gbps, massively improving upon the current 4G-LTE networks.

At the moment, the development of 5G systems splits itself into indoor and outdoor propagations. Generally, the sub-6 GHz range is applied to outdoor environments as it is easier to transmit and propagate, and communication companies (mainly in the United States and Asia) are already testing and applying 5G systems in this range for commercial purposes [2]. As the 5G sub-6 GHz mid-band has been established relatively recently, there are still many vacant frequencies throughout this range. Telecommunications regulatory agencies from various parts of the world – such as the FCC (Federal Communications Commission) in the United States, the METIS project (Mobile and wireless

communications Enablers for the Twenty-twenty Information Society 5G) in Europe [3], and Anatel (Telecommunications National Agency) in Brazil – are presently evaluating and auctioning unoccupied spectra for 5G applications. For the FCC, as evident in [4], mid-band frequencies are to be located at 2.5 GHz, 3.5 GHz and 3.7 to 4.2 GHz. According to Anatel, an auction of several frequencies was to be held in March 2020, aiming at the implementation of 5G systems in Brazil (the authors' home country). However, it has been postponed, and the new date is yet to be defined in 2021 [5]. Among the frequencies to be sold, there are: 700 MHz, 2.3 GHz, 3.3 GHz, 3.4 GHz and 3.5 GHz for outdoor systems [6].

The main advantage of the FSS proposed herein is that it is a multi-band device, with three distinct resonant frequencies in the S and C microwave range, according to IEEE classification. The novelty is that, despite its simple and passive filter implementation, it is possible to produce a multi-band response with the aid of a computational synthesis of the physical properties of the three conductive loops that characterize the device – blending, therefore, computational optimization and multi-band EM filter design through uncomplicated methods. The synthesis of the structure is produced with the hybridization of two computational methods: A general regression neural network (GRNN) and a multiobjective cuckoo search (MOCS) algorithm. This method takes the physical dimensions of the frequency selective surface (FSS) as inputs and three frequency bands at the output. As a stochastic network, the GRNN is significantly faster than ones depending on backpropagation, while still providing satisfactory accuracy. The MOCS is utilized to provide a search space in which the optimal solution (or solutions) can be found – this algorithm has been chosen due to its computational agility and multiobjective approach, as it is necessary to output more than one variable.

Therefore, the main objective of this study is to develop an FSS capable of operating at multiple bands, as well as multiple systems, within the sub-6 GHz range. As the proposed geometry contains a triple-resonance frequency response, the frequency spectrums near said resonances are bound to be within the structure's field of operation. Therefore, the main three bands chosen for the synthetic process of the FSS are: the 2.4 GHz Wi-Fi band (IEEE 802.11 standards), the 3.5 GHz 5G band [4]–[6] and the 5.8 GHz WiMAX band (IEEE 802.16 standards). In this case, the secondary objective of the proposed device is to tune it into the 5G mid-band frequencies as best as possible, within the boundaries of the three main resonant frequencies. As such, the following bands should also become attainable: 2.3 GHz, 2.5 GHz, 3.4 GHz, 5.5 GHz (a WLAN band) and 6 GHz.

The paper is presented in the following order: Section 2 explains the chosen geometry for the single-layered FSS, exposing its physical parameters; in Section 3, an explanation of the hybrid, bioinspired optimization method GRNN+MOCS is provided; Section 4 discourses on the optimization technique's results, as well as the simulated and measured ones for the FSS; to finalize, Section 5 holds the conclusion of the study.

II. STRUCTURE OF THE DEVICE

The FSS herein proposed presents a rectangular unit cell, as well as three rectangular loop patches. This geometry has been selected due to its simple design, being able to achieve a steady multiband response whilst evenly occupying the unit cell with easy-to-build physical parameters.

For both current and future means of mobile information transmission, electromagnetic (EM) filtering is ever so greatly necessary. Due to the high number of channels and density of communication systems,

different broadcasting and propagating spectra can be, in many cases, very proximate to each other. These filters act as signal barriers and interference reducers for crossing EM signals – thus resulting in better quality of reception and transmission. Frequency Selective Surfaces are EM filters presenting one or multiple unit cell conductive patterns arranged periodically onto a surface - commonly on substrate plates or wallpapers. Depending on the geometrical composition of the unit cell, distinct electromagnetic behaviors can be observed.

Many examples of multi-band FSS response already exist in the literature, although most of these devices require dual-layering, multiple unit cells and / or active elements to be incorporated into its design – such complex properties that the simpler-to-build FSS model proposed herein does not possess, e.g. [7]–[9]. There are also many arbitrarily-designed devices for multi-frequency operation, such as [10], [11], in which there is minimum information about the proposed FSS and no metaheuristic optimization in order to facilitate and validate the structure’s design. And for the examples on FSS synthesis by a computational method, few are the ones that present multi-band filtering [12]–[14].

As previously said, many studies on FSS in the literature demand more complex and costly design techniques to yield a multiband response, such as mixture of unit cells, active switching components and / or dual-layering [7]–[9]. Hence, the single-layer, single-pattern unit cell and single-plate design of the FSS displayed in this section is objectively a simpler solution to produce a tri-band frequency response cost-wise, modelling-wise and construction-wise. Fig. 1 depicts the design of the unit cell.

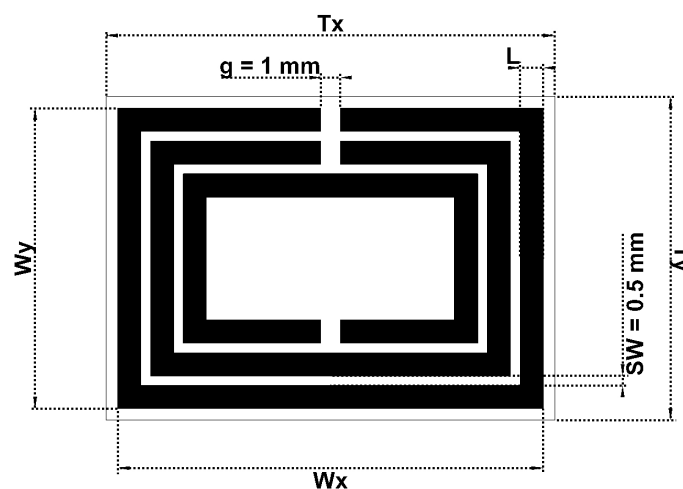


Fig. 1. The device’s unit cell design.

Structural parameters of the triple rectangular loop FSS utilized in its synthesis are listed in Table I. These are: the unit cell’s horizontal and vertical dimensions (T_x and T_y) and the width of the loops (L). Below them, other constant physical values of interest are denoted, such as the spacing between the rectangular loops (SW) and the gaps present within the loops (g). These search space bounds of the optimization have been fairly estimated taking into account the numerical analysis for squared loop band-stop filtering present in [15], separately for each of the three loops on the unit cell.

The L parameter stands for both the width of each loop (which is of equal value for all three patches) and the difference between the outermost loop patch and the unit cell’s boundaries, as defined by (1).

TABLE I. PHYSICAL PARAMETERS OF THE UNIT CELL

Parameters	Values (in millimeters)
Horizontal size (Tx)	[23, 23.5, 24, 24.5, 25]
Vertical size (Ty)	[16, 16.5, 17, 17.5, 18]
Loop width (L)	[1.2, 1.3, 1.4, 1.5]
Loop spacing (SW)	0.5
Loop gap (g)	1
Substrate thickness	1.57

$$L = T_x - W_x; L = T_y - W_y \quad (1)$$

Being that W_x and W_y are dependent variables – by the manner in which the device is intrinsically designed – these are not necessary to the training of the GRNN, thus diminishing computational effort by creating a linear correlation to two independent variables that are already employed into the neural network.

The gaps (g) in the loops act as fine-tuning for the resonant frequencies of the structure, held at a constant value of just 1 millimeter wide. The spacing between the patches is set to a minimum value of 0.5 millimeter, both vertically and horizontally, as values lower than this may cause the structure to have parameters too small to construct, and values above the aforementioned may draw the resonant frequencies too far apart from each other in the frequency response.

Fig. 2 exposes the constructed FSS. An epoxy glass FR-4 single-layer plate is used as the substrate, 20 x 25 centimeters long, with a thickness of exactly $h = 1.57$ mm. The etching of the conductor layer to the board has been made by ferric chloride corrosion. According to CST® Microwave Studio, the software utilized for all simulations present in this paper, the values of electromagnetic properties worth noting for this substrate are the relative permittivity of $\epsilon_r = 4.4$, and loss tangent of $\sigma = 0.025$ at 10 GHz.

III. THE GRNN-MOCS OPTIMIZATION METHOD

Bioinspired algorithms are good optimization tools for solving Engineering and Mathematical problems, particularly those that trial-and-error methods (metaheuristics) may be applied to solve practical problems. As an example of such metaheuristic optimization, there is the Multiobjective Cuckoo Search (MOCS) algorithm utilized in this study [16].

The synthesis process of an FSS is characterized as the parametrization and optimization of its cell geometry through a given optimization technique. Many examples of the synthetical process of FSS design are currently found in the literature. For example, there are studies that apply Genetic Algorithms (GA) [17]–[19], Particle Swarm Optimization (PSO) [13], [20], Bat Echolocation Algorithm (BA) [21] and the Flower Pollination Algorithm (FPA) [22] for the sake of performing said synthesis. Most of these applications employ a hybrid method involving backpropagation-based ANNs.

Even though these methods are all tried-and-true solutions, the optimization process may still spend hours, or even days, of computational time to train the neural networks. With this in mind, there is a considerable amount of time reduction if the GRNN-MOCS hybrid method is utilized, as evident in [14] – producing a faster result while keeping a high level of accuracy.

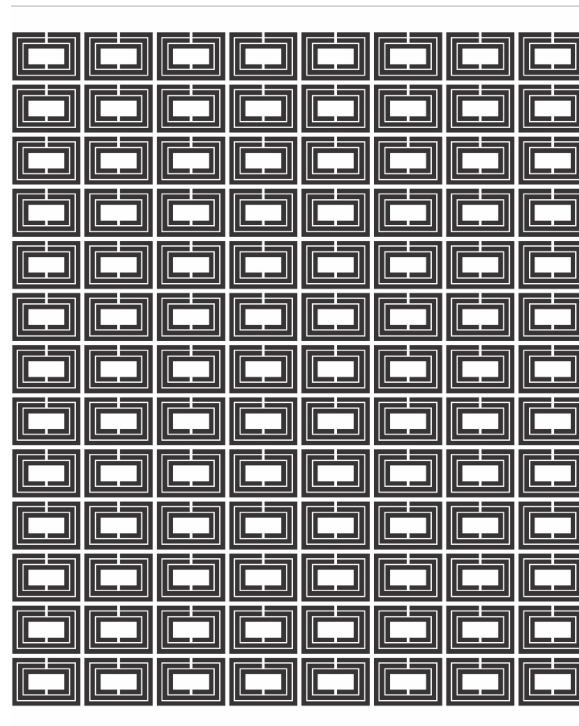


Fig. 2. FSS imprinted upon an FR-4 glass epoxy substrate.

A. Theory and Hybridization of GRNN and MOCS

The General Regression Neural Network, in the form that is modelled currently, has been introduced by E. Specht in 1991 [23]. It is a probability-based ANN that requires no backpropagation for data training, as only a fraction of the database is actually necessary to the training process.

The GRNN is a stochastic network, specifically fitting into the Radial Base Function group (RBF), because its definition and development start from a distribution function and a conditional mean value of the output, in relation to the input [24]. This conditional mean is what gives the network its name, since it is a process of regression of the output Y, given that an X input was already brought upon the system.

In order to calculate said regression, there are two whole sums that gather the output values of the final layer and convert such data into the numerator and denominator of the distribution function. This fraction's result provides the value of the output after the regression has been concluded. As stated by the definitions of [23], along with the application shown in [14], an activation function exponentially defined and its output are given by Eqs. 2 and 3:

$$g_i = \exp\left(-\frac{D_i}{2\sigma^2}\right) \quad (2)$$

$$Y(X) = \frac{\sum_{i=1}^n Y_i \exp\left(-\frac{D_i}{2\sigma^2}\right)}{\sum_{i=1}^n \exp\left(-\frac{D_i}{2\sigma^2}\right)} \quad (3)$$

In which σ is the density interpretation that the neural network should represent, also called the smoothness parameter. For values of σ that are closer to zero, the density estimate might turn into a non-gaussian response, and if the values are too great the density becomes fully gaussian and greatly

smoothened, producing a $Y(X)$ that is the result of the average value of all output samples Y_i . And D_i is the distance between a training sample X_i and the result prediction estimate X – this equation is represented as such:

$$D_i^2 = (X - X_i)^T (X - X_i) \quad (4)$$

The cuckoo search metaheuristic algorithm, first planned by Yang and Deb in 2009 [25], proves to be very useful and effective for many applications in the fields of mathematics, engineering and industry [26]. The bioinspiration behind it is the parasitic behavior of birds of the cuckoo family, that lay their eggs inside the nests of other species of birds.

In 2013, the authors of the original CS algorithm adapted its approach to allow for multiobjective computation, thus creating the Multiobjective Cuckoo Search (MOCS) [16]. Given that the FSS proposed in this study possesses three different frequency band objectives, MOCS is the search space method chosen to be utilized. There are three rules, as stated by the creators, that define this algorithm:

- Each cuckoo lay k eggs (solutions for the objective functions) at a time, and deposits them in a random nest N . Each egg is considered a potential solution – metaheuristic
- The best nests carry the best eggs (solutions), and these will survive the next generations due the parasitic nature of the cuckoo hatchlings – elitism.
- The number of available nests is constant, and defined by the code developer. The probability of N nest being discovered by the host bird is defined as $Pa \in [0, 1]$. After this, the bird may choose to discard the eggs or abandon its nest – discarding the worst solutions.

The cuckoo birds in this method move according to the so-called Lévy Flights [25]. This device provides a random flight path that which each cuckoo (in a number of i cuckoo birds) will trek to find nests. Equations (5) and (6) are a mathematical representation of the Lévy Flight and Lévy Distribution, respectively, to be implemented in code form:

$$x_i^{t+1} = x_i^t + \alpha \oplus Levy(\beta) \quad (5)$$

$$Levy(\beta) \cong u = t^{-(\beta+1)}; (1 < \beta \leq 3) \quad (6)$$

in which i is the maximum number of cuckoo birds in the current generation, and t is the current code iteration. Constant α is the step size to be utilized in the code, and is adaptable to the developer's need – it must always be greater than zero. The β constant is related to the distribution of the random walks in the flights, in which an intermediate value has been chosen. In this study the values are set to $\alpha = 1$ and $\beta = 1.5$.

Multiobjective optimization evaluate results through a Pareto Front (or Pareto Frontier) – that is, a reference region of optimal values that the outputs must achieve. Thus, in a code that implements the MOCS, a comparison with the Pareto Front is usually made from the best solutions obtained in the search space.

A pseudocode of the MOCS algorithm can be found in the article in which it was proposed by Yang and Deb [16].

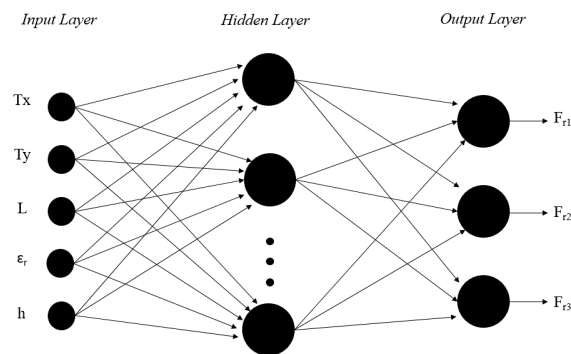


Fig. 3. Scheme of the GRNN utilized for the optimization.

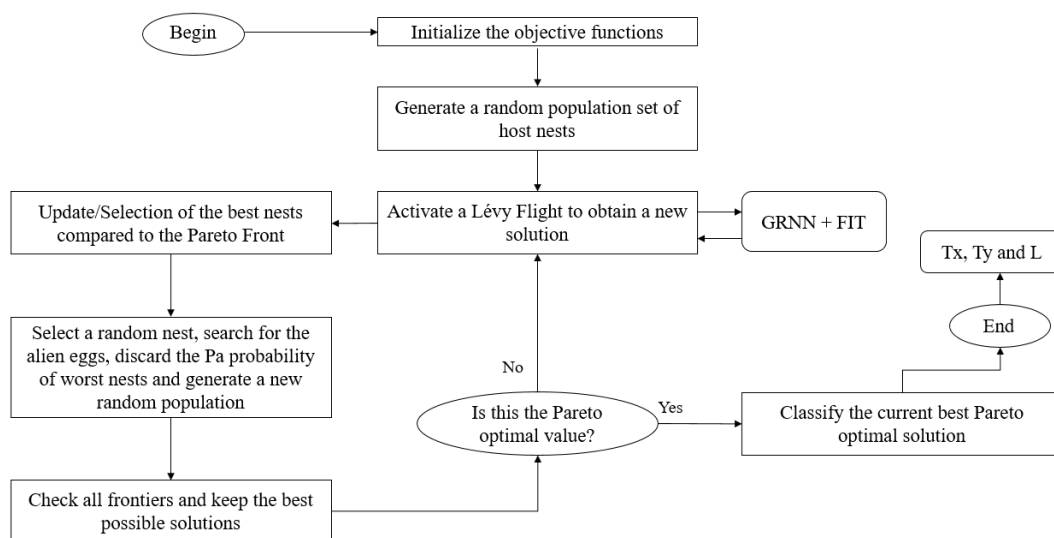


Fig. 4. Flowchart of the GRNN-MOCS optimization method.

The blending of a general regression neural network (GRNN) with the cuckoo search (CS) algorithm is a bioinspired, metaheuristic solution to problems that require quicker but robust solutions, good accuracy and lesser computational effort – mainly for the areas of engineering and mathematics. The main objective of this technique is to reduce drastically the training time necessary for the neural network to train itself, with the aid of the multiobjective cuckoo search, that searches for the best possible solutions in each iteration of the code.

The training set has been acquired through the Finite Integrations Technique (FIT) numerical analysis, given that it is the analytical tool employed by the chosen computational simulator.

Table I denotes the three input parameters and its discrete values utilized as training data for the ANN, as well as its two biases: $\epsilon_r = 4.4$ and $h = 1.57$, and the schematic for the GRNN implemented is shown in Fig. 3. A flowchart of the optimization method is illustrated in Fig. 4.

As the training process is completed, the GRNN will generate a Region of Interest (ROI), in which the MOCS search algorithm seeks out the best possible solutions to the objective functions. Thus, for every set of parameters the search algorithm returns to the network, a phase of calculation and analysis takes place to determine the values of a new point within the search space.

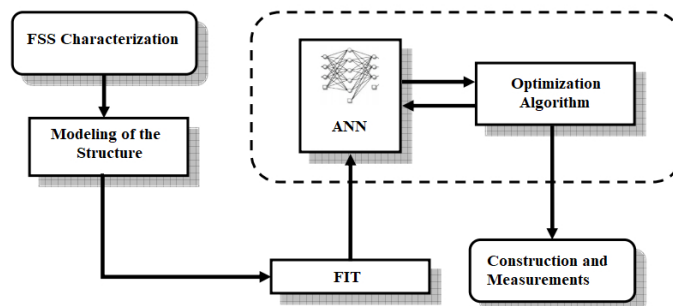


Fig. 5. Overview flowchart [22].

The construction of the training data and the optimization process has been executed in a laptop computer, possessing an Intel® Core i5 2.5 GHz CPU and 8 GB of RAM.

The configuration of the GRNN applied to this study presents five input neurons (three variables and two biases), a hidden layer of five neurons, and three output cells. The outputs are the three resonant frequencies set as the bands of interest for the FSS operation, that is: 2.4 GHz, 3.5 GHz and 5.8 GHz. Fig. 3 illustrates the schematic of the utilized neural network.

Fig. 5 shows a flowchart of all steps made in this study, utilizing the process evident in [22].

B. Computational Results

The inputs and outputs of the neural network can be represented as:

$$x = [T_x, T_y, L, \epsilon_r, h]^T \quad (7)$$

$$y = [f_{r1}, f_{r2}, f_{r3}]^T \quad (8)$$

In which Eq. (7) denotes the T_x and T_y unit cell geometry dimensions (in the x and y axis, respectively) and the width of the loops L . The ϵ_r and h constant inputs are fixed properties of the structure and may be used as biases to regulate the GRNN. Eq. (8), in the other hand, represents the three resonant frequency outputs of the device: f_{r1}, f_{r2}, f_{r3} .

The objective function (or cost function) is as such:

$$F = [f_1(x), f_2(x), f_3(x)] \quad (9)$$

Which is equated to attend these demands:

$$f_1 = |f_{r1desired} - f_{r1obtained}| \quad (10)$$

$$f_2 = |f_{r2desired} - f_{r2obtained}| \quad (11)$$

$$f_3 = |f_{r3desired} - f_{r3obtained}| \quad (12)$$

The desired frequency bands of operation are, respectively: 2.4 GHz, 3.5 GHz and 5.8 GHz. Thus, the minimal fitness level is calculated as the sum of the values of objective functions f_1 , f_2 and f_3 as such:

$$f_{min} = (f_1 + f_2 + f_3) \quad (13)$$

A total of 100 data training points has been acquired through the FIT simulation executed with CST® Microwave Studio 2018. The running time of the GRNN training code including all 100 calls – written in Matlab® – has clocked at only 4.32 seconds, as stated in Table II.

Fixed parameters for the GRNN-MOCS method involve the fixed upper and lower boundary values of the optimization’s search space, representing variables T_x , T_y and L, respectively: $P_{min} = [23; 16; 1.2]$ and $P_{max} = [25; 18; 1.5]$. Also, there is a set of constants defined to run the multiobjective cuckoo search properly, such as total number of concomitant nests (or solutions) equal to $n = 25$, with an alien egg discovery rate of $P_a = 0.25$, the scalar vector $\beta = 1.5$ and a fraction of 0.7 of the Pareto Frontier to be analysed for the acquisition of best solutions. Furthermore, the algorithm has been limited to a total of 1000 iterations.

Fig. 6 denotes fitness values for the synthesis of the triple-loop rectangular patch FSS. At the y-axis, there is the value of the cost function (in which smaller values are better), and at the x-axis is the iteration count. It is noticeable the diminution of the cost function value as the iteration count increases, and it continues to decline until a moment in which the cost function is very close to zero. The dashed line represents the average fitness value for all results, whilst the solid line is the best possible solution.

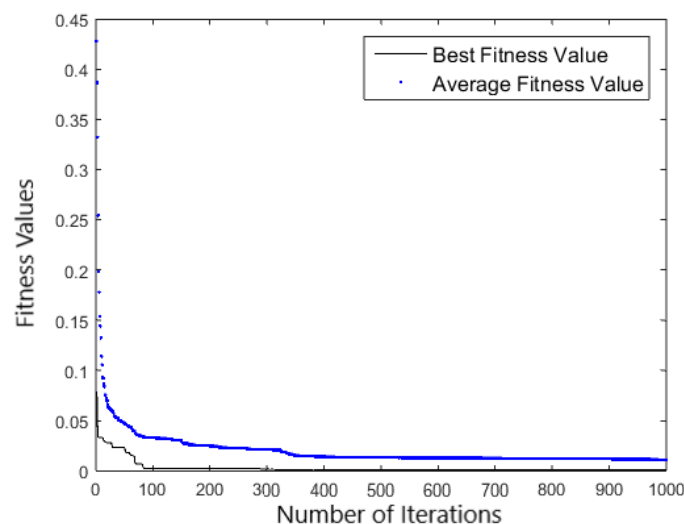


Fig. 6. Fitness values for the GRNN-MOCS implementation.

TABLE II. Running times for the GRNN-MOCS configured at $N = 25$ and 1000 iterations

Optimization Stage	Calls	Time (in seconds)
GRNN Training	100	4.324
MOCS	50025	719.258

As said previously, a total of 1000 iterations were necessary to accomplish convergence at a cost function value of only $f_{min} = 4.7 \times 10^{-4}$. The entire process has lasted less than 12 minutes (719.258 seconds) for a high number of iterations (1000), which characterizes an efficient and fast optimization option for multiband FSS. Table 2 informs the number of calls and the total time taken for both the neural network training and the GRNN-MOCS optimization process.

The exact dimensions found by the hybrid method are such: $T_x = 23.26mm$; $T_y = 16.76mm$; and $L = 1.2mm$.

IV. MEASUREMENTS AND RESULTS

The experimental and FSS construction phases have been conducted at the Microwaves Laboratory of the Group of Telecommunications and Applied Electromagnetism (GTEMA), resident within the Federal Institute of Education, Science and Technology of Paraíba, Brazil (IFPB). An Agilent E5071C two-port network analyser and two pairs of horn-type antennas (SAS-571 from 0.7 - 18.0 GHz) were used for the measurements. The antennas were 1.2 metre apart, at an angle of 180° to each other. An FSS support setting was also used to maintain the device between the antennas. At the lower part of the support, there is a guide ruler, employed in the precise determination of the angle at which the FSS is placed in relation to the antennas. This makes possible to change wave incidence angle on the filter, in order to verify its angular phase stability. In this study, the designed device has been subjected to angular phase stability tests for the following angles: $\theta = 0^\circ, \theta = 15^\circ, \theta = 30^\circ$ and $\theta = 45^\circ$. Fig. 7 illustrates the measuring setup, as well as the network analyser.

Fig. 8a illustrates the plotted simulated results of CST® software compared to the measured frequency response of the FSS. Whereas Fig. 8b denote measured results for the incidence angles of $\theta = 0^\circ, \theta = 15^\circ, \theta = 30^\circ, \theta = 45^\circ$.

It can be denoted that the frequency response up until $\theta = 45^\circ$ is satisfactory to operate between the objective frequencies planned in this work. Higher values of wave incidence angles do not show an equivalency between simulated and measured values, and so have been discarded from the plots. Table III denotes the differences in resonance (Fr) and bandwidth (BW) between the simulated optimised results and the physically measured results of the FSS, considering a wave incidence angle of $\theta = 0^\circ$.

TABLE III. FREQUENCY RESPONSE COMPARISON (IN GHZ)

Set	$[F_{r1}, F_{r2}, F_{r3}]$	$[BW_1, BW_2, BW_3]$
Simulated	[2.36, 3.48, 5.70]	[0.66, 0.25, 0.99]
Measured	[2.53, 3.61, 5.90]	[0.48, 0.32, 0.97]

A. Surface Current Simulations

One of the intentions of the FSS proposed in this paper is to produce a three-band frequency response, and the method chosen to reach such claim has been to synthesise three rectangular loops, so that each one shall accommodate a specific resonant frequency. Therefore, the outermost loop presents its peak surface current at the lowest resonance, that is 2.4 GHz, in which the two other loops present very little surface current density at this spectrum, as attested in Figure 9a. In an analogous way, the middle loop produces the 3.5 GHz resonance (Fig. 9b) and the innermost loop is the main resonator at 5.8 GHz (Fig. 9c). These simulations have been conducted in software CST® Microwave Studio 2018.

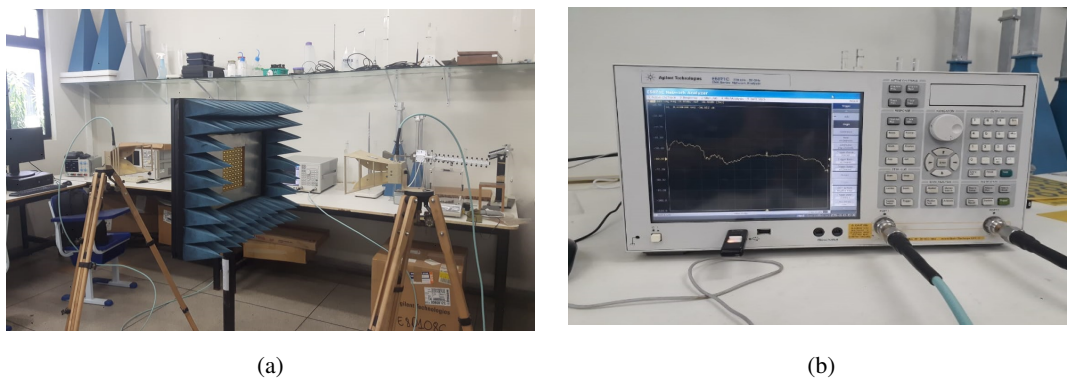
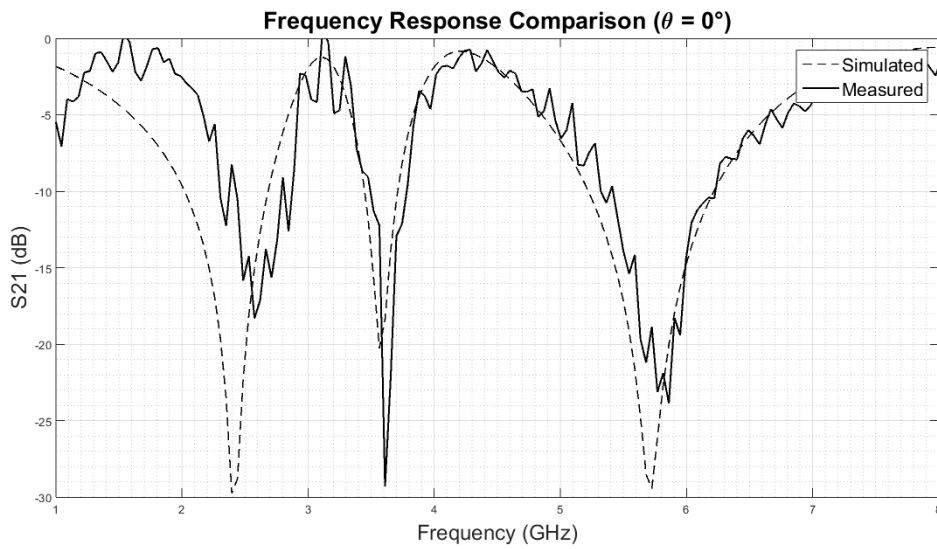
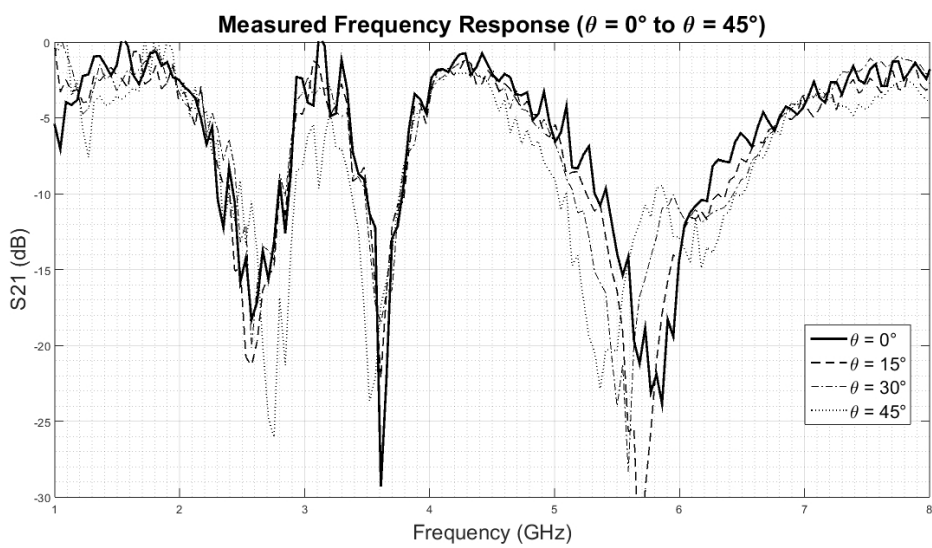


Fig. 7. Setup and Equipment: (a) Horn-type antennas and the FSS support; (b) Network analyser.



(a)



(b)

Fig. 8. Frequency responses of the FSS device: (a) Simulated and measured results for $\theta = 0^\circ$; (b) Measured results up until $\theta = 45^\circ$.

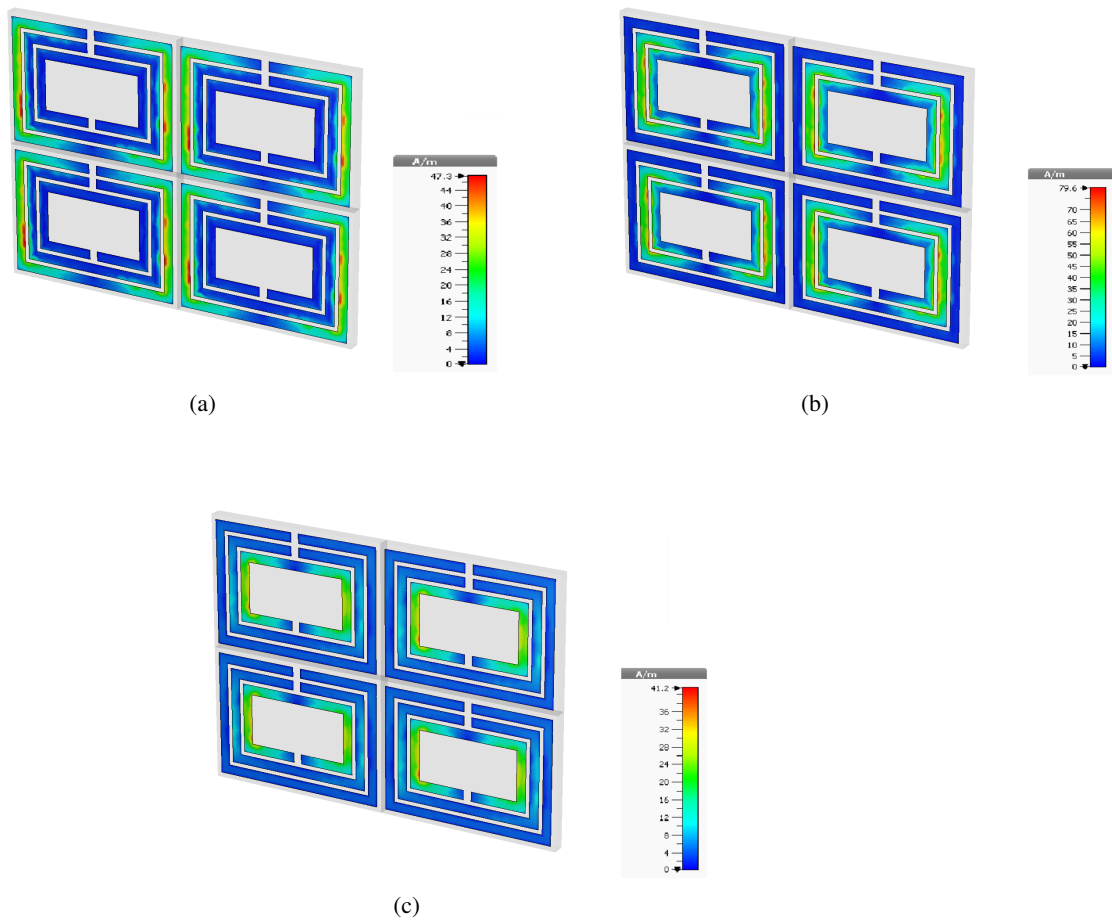


Fig. 9. Surface currents for all resonances of the FSS device: (a) Resonance at 2.4 GHz (peaks at 47.3 A/m); (b) Resonance at 3.5 GHz (peaks at 79.6 A/m); (c) Resonance at 5.8 GHz (peaks at 41.2 A/m).

V. CONCLUSION

In this study, the simulation, synthesis and construction of an EM structure in the form of a multi-band frequency selective surface is explored. It was proposed herein, as a means of achieving multi-band performance, the unit cell geometry of triple-loop rectangular patches.

A triple-resonance response has been reached with a simple, common substrate plate made of glass epoxy (FR-4), thus increasing the capability of construction of the device in low-cost conditions. However, it is important to state that the precision of the conductive layer etched onto the plate must not greatly deviate from the optimal dimensions - especially for the parameter of spacing between loops of only 0.5 millimeters. So, a high-precision printer may be required for obtaining high accuracy in the results.

The GRNN has been very effective in computational cost and agility, denoting fast results with only 100 training points for the structure. The MOCS algorithm has performed its search duties also in a significant fast way, considering that a total of 1000 iterations have been performed (this value was fixed as the author's choice) producing a minimal fitness value in the order of 10^{-4} , which is more than enough to provide solid results for the synthesis of the FSS within the objective spectrums of 2.4, 3.5 and 5.8 GHz.

The frequency responses obtained in this study, for this structure, also successfully envelop the spectrums of 2.3, 2.5, 3.4, 3.5, 5.5 and 6 GHz, remaining below -10 dB for all of these bands. That is, the device can prove itself to become a useful tool for future 5G propagation systems. The fact that the FSS also supports operation in popular Wi-Fi, WLAN and WiMAX bands makes it a robust, multiuse, "jack of all trades" EM filter.

ACKNOWLEDGMENTS

The authors would like to thank the support of National Council for Scientific and Technological Development (CNPq), the National Institute of Science and Technology in Wireless Communication (INCT-CSF), Coordination of Superior Level Staff Improvement (CAPES), Group of Telecommunications and Applied Electromagnetism (GTEMA) of the Federal Institute of Education, Science and Technology of Paraíba (IFPB) and the Federal University of Pará (UFPA).

REFERENCES

- [1] E. Dahlman, G. Mildh, S. Parkvall, J. Peisa, J. Sachs, and Y. Selén, "5g radio access," *Ericsson review*, vol. 6, no. 1, 2014.
- [2] J. Lee, E. Tejedor, K. Ranta-aho, H. Wang, K.-T. Lee, E. Semaan, E. Mohyeldin, J. Song, C. Bergljung, and S. Jung, "Spectrum for 5g: Global status, challenges, and enabling technologies," *IEEE Communications Magazine*, vol. 56, no. 3, pp. 12–18, 2018.
- [3] H. Tullberg, P. Popovski, Z. Li, M. A. Uusitalo, A. Høglund, O. Bulakci, M. Fallgren, and J. F. Monserrat, "The metis 5g system concept: Meeting the 5g requirements," *IEEE Communications magazine*, vol. 54, no. 12, pp. 132–139, 2016.
- [4] F. C. Commission, *The FCC's 5G FAST Plan*, 2018 (accessed 17 July, 2020). [Online]. Available: <https://www.fcc.gov/5G>
- [5] M. Brown, *5G Public Auction in Brazil*, 2009 (accessed 17 July, 2020). [Online]. Available: <https://www.mayerbrown.com/en/perspectives-events/publications/2020/06/5g-public-auction-in-brazil>
- [6] Bnamericas, *Brazil pencils in 5G auction for 2020*, 2019 (accessed 17 July, 2020). [Online]. Available: <https://www.bnamericas.com/en/news/brazil-pencils-in-5g-auction-for-2020>
- [7] H. Luo, W. Wu, S. Xie, J. Fan, and N. Yuan, "Multiband fss with wideband and sharp falling down characteristics," *Microwave and Optical Technology Letters*, vol. 58, no. 2, pp. 378–382, 2016.

- [8] B. Rahmati and H. Hassani, "Multiband metallic frequency selective surface with wide range of band ratio," *IEEE Transactions on Antennas and Propagation*, vol. 63, no. 8, pp. 3747–3753, 2015.
- [9] H. Li, Q. Cao, L. Liu, and Y. Wang, "An improved multifunctional active frequency selective surface," *IEEE Transactions on Antennas and Propagation*, vol. 66, no. 4, pp. 1854–1862, 2018.
- [10] N. Choudhary, A. Sharma, and S. Yadav, "A novel band stop frequency selective surface for the security of quad band mobile applications," in *2017 IEEE Applied Electromagnetics Conference (AEMC)*, pp. 1–2, 2017.
- [11] S. Yadav, C. P. Jain, and M. M. Sharma, "Smartphone frequency shielding with penta-bandstop fss for security and electromagnetic health applications," *IEEE Transactions on Electromagnetic Compatibility*, vol. 61, no. 3, pp. 887–892, 2018.
- [12] P. Oliveira, A. D'Assunção, E. Souza, and C. Peixeiro, "A fast and accurate technique for fss and antenna designs based on the social spider optimization algorithm," *Microwave and Optical Technology Letters*, vol. 58, no. 8, pp. 1912–1917, 2016.
- [13] M. Panda and P. P. Sarkar, "Prediction of periodicity of fss structure using particle swarm optimization," *i-Manager's Journal on Electronics Engineering*, vol. 7, no. 3, p. 25, 2017.
- [14] M. A. Neto, J. Araújo, F. Barros, A. Silva, G. Cavalcante, and A. d'Assunção, "Bioinspired multiobjective synthesis of x-band fss via general regression neural network and cuckoo search algorithm," *Microwave and Optical Technology Letters*, vol. 57, no. 10, pp. 2400–2405, 2015.
- [15] K. R. Jha, G. Singh, and R. Jyoti, "A simple synthesis technique of single-square-loop frequency selective surface," *Progress In Electromagnetics Research B*, vol. 45, pp. 165–185, 2012. [Online]. Available: <http://www.jpier.org/PIERB/pier.php?paper=12090104>
- [16] X.-S. Yang and S. Deb, "Multiobjective cuckoo search for design optimization," *Computers & Operations Research*, vol. 40, no. 6, pp. 1616–1624, 2013.
- [17] W. G. Lima, J. P. L. de Araújo, F. J. Brito, L. Castro, and M. C. de Alcântara Neto, "Optimization and synthesis of multilayer frequency selective surfaces via bioinspired hybrid techniques," *International Journal for Innovation Education and Research*, vol. 8, no. 5, pp. 541–562, 2020.
- [18] L. Lanuzza, A. Monorchio, and G. Manara, "Synthesis of high-impedance fsss using genetic algorithms," in *IEEE Antennas and Propagation Society International Symposium (IEEE Cat. No. 02CH37313)*, vol. 4, pp. 364–367, 2002.
- [19] A. Campos, A. Martins, and V. Almeida Filho, "Synthesis of frequency selective surfaces using genetic algorithm combined with the equivalent circuit method," *Microwave and Optical Technology Letters*, vol. 54, no. 8, pp. 1893–1897, 2012.
- [20] S. Genovesi, R. Mittra, A. Monorchio, and G. Manara, "Particle swarm optimization for the design of frequency selective surfaces," *IEEE Antennas and Wireless Propagation Letters*, vol. 5, pp. 277–279, 2006.
- [21] M. C. Neto, J. P. Araújo, R. J. Mota, F. J. Barros, F. H. Ferreira, G. P. Cavalcante, and B. S. Castro, "Design and synthesis of an ultra wide band fss for mm-wave application via general regression neural network and multiobjective bat algorithm," *Journal of Microwaves, Optoelectronics and Electromagnetic Applications*, vol. 18, no. 4, pp. 530–544, 2019.
- [22] M. C. de Alcântara Neto, H. R. O. Ferreira, J. P. L. de Araújo, F. J. B. Barros, A. G. Neto, M. de Oliveira Alencar, and G. P. dos Santos Cavalcante, "Compact ultra-wideband fss optimised through fast and accurate hybrid bio-inspired multiobjective technique," *IET Microwaves, Antennas & Propagation*, 2020.
- [23] D. F. Specht *et al.*, "A general regression neural network," *IEEE transactions on neural networks*, vol. 2, no. 6, pp. 568–576, 1991.
- [24] S. Haykin, *Neural networks: a comprehensive foundation*. Prentice-Hall, Inc., 2007.
- [25] X.-S. Yang and S. Deb, "Cuckoo search via lévy flights," in *2009 World congress on nature & biologically inspired computing (NaBIC)*, pp. 210–214, 2009.
- [26] S. Kamat and A. G. Karegowda, "A brief survey on cuckoo search applications," *Int. J. Innovative Res. Comput. Commun. Eng.*, vol. 2, no. 2, 2014.